Observations and modelling of rotational signals in the P-Coda: constraints on crustal scattering

by N. D. Pham, H. Igel, J. Wassermann, M. Käser, J. de la Puente, U. Schreiber

Corresponding Author:

Heiner Igel

Geophysics Section, Department of Earth and Environmental Sciences, LMU Munich,

Theresienstr. 41, 80333 Munich, GERMANY.

Room: 440

Phone: +49 (89) 2180-4204

Fax: +49 (89) 2180-4205

Email: heiner.igel@geophysik.uni-muenchen.de

Abstract

In addition to three classical components (vertical, N-S, and E-W) of ground translations recorded by broadband seismometer, the vertical component of earthquake induced rotational ground motions is consistently measured by a ring laser sensor located in Wettzell, SE Germany. Significant rotational motions in the P coda of tele-seismic signals are either directly visible or can be inferred through the investigation of cross-correlation between transverse acceleration and vertical rotation rate. Theoretically, in spherically symmetric isotropic media we should not observe a vertical component of rotations before the onset of SH waves. Possible causes for the observed rotations in the P coda are: (1) tilt – ring laser coupling; (2) anisotropy; (3) topographic scattering; and (4) P-SH scattering in the crust. Here we show that P-SH scattering in the 3D random crust can explain the observations and allow us to constrain crustal scattering properties.

Introduction

In seismology, observations are traditionally based on measurements of inertial seismometers that record three components (vertical, N-S, and E-W) of earthquake induced ground translations (displacement, velocity, or acceleration). There are theoretical studies suggesting that in addition to translations, rotational ground motions should be measured (e.g., Aki and Richards, 2002). This type of observation might be relevant for: (1) correcting translation signals recorded by classical seismometers for contamination by ground rotation (Graizer, 2005; Graizer, 2006; Pillet and Virieux, 2007); (2) extracting additional information on earthquake source properties (e.g., Takeo and Ito, 1997; Takeo, 1998), soil - structure – interactions (Trifunac and Todorovska, 2001), and properties of the subsurface (Igel et al., 2007; Fichtner and Igel, 2008); (3) providing additional ground motion information to earthquake engineers for seismic design (e.g., Li et al., 2001, 2002). However, the lack of instrumental resolution did not allow seismologists to record this kind of motions in a consistent way until recently (Pancha et al., 2000; Schreiber et al., 2005; Cochard et al., 2006; Igel et al., 2005, 2007).

Ring laser technology has provided the means to allow in principle observation of rotational motions in a wide frequency band and epicentral distance range (Schreiber et al., 2005; Igel et al., 2005, 2007). The remarkable consistency between rotational ground motions around a vertical axis recorded by ring laser and transverse acceleration for periods of 1s up to 150s and suitable values of the phase velocities estimated by taking the ratio of transverse acceleration and rotation rate are not only proving the appropriateness of the ring laser sensor but also imply that the multi-component observations allow the estimation of wave field properties (e.g. phase velocities, propagation direction) that otherwise are only accessible with high accuracy through array measurements (Igel et al., 2007).

In a previous study (Igel et al., 2007), a significant rotational motion component in the P coda of seismic signals had been recognized. At first, this is a surprising observation because, theoretically, in spherically symmetric isotropic media P and SV waves do not generate a vertical component of rotation so we should not observe this kind of motions before the arrival times of SH waves. There are several possible explanations for the phenomenon of P coda rotations: (1) tilt – ring laser coupling: when P waves arrive they do generate tilts at the Earth's surface (i.e. rotational motions around horizontal axes). This will contaminate the ring laser measurements through changes of the surface normal with respect to the Earth's rotation axis and may potentially contribute to the phenomenon of rotation in the P coda (Schreiber et al., 2005; Igel et al., 2007); (2) P-SH scattering in the crust; (3) anisotropy; and (4) topographic scattering. The tilt – ring laser coupling is assumed to be small in the far field case (McLeod et al., 1998; Igel et al., 2007). We detail and further systematically investigate this in a companion paper (Pham et al., 2008). In this study this effect is assumed negligible. The contributions of anisotropy and topographic scattering on the P coda rotations are expected to be small but were never properly quantified. This will be the subject of a future study. Here, we focus on investigating the effects of P-SH scattering in the crust on the vertical component of rotational ground motions.

The main goals of this study are to present the observations of rotational motions around a vertical axis in the P coda, and to model these observations with 3D wave propagation through random crustal media.

Observations

Database

The data used in this study includes collocated records of both the G - ring laser sensor and broadband seismometer (STS-2) at the Fundamental station, Wettzell, SE-Germany (see Data and Resources Section). The G - ring laser sensor is located in a purpose-built observatory and installed on an extremely stiff material (to avoid effects of temperature, pressure or deformation) and records rotational ground motions around a vertical axis. About 300 m away from this instrument, a STS-2 broad - band sensor (WET station, Lat. 49.15^0, Lon. 12.88^0, German Regional Seismic Network) records permanently three orthogonal components of ground velocity. Further details on the instruments and the measurement principle can be found in (Schreiber et al., 2006; Igel et al., 2007).

Observations of thirty-six earthquakes that occurred between 2003 and February 2008 are used in this study. The epicentral distance and magnitude distributions of the observed events are shown in Figure 1 with event information summarized in Table 1. Each event in this database includes 4 components recorded by the above-mentioned instruments: three traditional components of ground velocity and one vertical component of ground rotation rate. Transverse acceleration, another component usually used in this study, is inferred by rotating (in a local radial-transverse system) the time-differentiated components of the observed horizontal ground velocities.

In the following we investigate the observed P coda rotations systematically by examining their energy variations as a function of frequency, incoming direction, and time. The frequency and directional dependence of the P coda rotations is revealed using filtering and cross-correlation techniques. Normalized envelopes are used to investigate time-dependent variations of energy in the P coda rotations.

Frequency dependence of direct observations

Analysis of the observed data showed that in strong (or near) events the signals of the rotation rate are visible in the P coda sections. A typical example for these direct observations is the case of the Sumatra earthquake 12-09-2007, M8.4. To examine the frequency dependence of the P coda rotations, we low-pass filter the signals with different cut-off periods. Results are shown in Figure 2. We observe that with increasing cut-off period, the amplitude of the P coda rotations is decreased. Amplitudes of the P coda rotational signals decrease significantly for a cut-off period T=5s and almost disappear when the cut-off period reaches a value of 10s. This implies that the energy of the observed P coda rotations is predominant at high frequencies. This phenomenon is observed for all events with visible P-coda rotations.

Increase in correlation right after the onset of P wave

As indicated in Table 1, in many cases rotational energy in the P coda is hidden in the noise. An example is shown in Figure 3. The Al Hoceima event 24-02-2004, M6.4, does not show visible P coda rotations (Figure 3, the third trace from top). To investigate the variation of rotation rate in such events, we use the cross - correlation technique. Theoretically, assuming plane shear-wave propagation in horizontal direction with transverse polarization, rotation rate and transverse acceleration should have the same waveform and their amplitudes should scale proportionally to two times the phase velocity (Cochard et al., 2006; Igel et al., 2005, 2007). In the P - coda time window, with clear visibility of transverse acceleration, an increase of correlation between rotation rate and transverse acceleration would therefore indicate the presence of (scattered) SH energy, because (as mentioned before) P and SV waves do not generate a vertical component of rotation. The zero lag normalized cross-correlation coefficient - defined between 0 (no similarity) and 1 (perfect match) - between rotation rate and transverse

acceleration was calculated for a sliding time windows of appropriate length (twice the dominant period) along the time series. After high-pass filtering both signals (transverse acceleration and rotation rate) with cut-off period T=1s, using 2s sliding time window, the results reveal a clear increase of the coefficients right after the onset of P (Figure 3, bottom). The same processing for all events in the period 2003-2004 shows a clear increase of the correlation coefficients between high-pass filtered rotation rate and high-pass filtered transverse acceleration at (and following) the onset of P waves for all events (Figure 4). This result indicates the existence of high frequency P coda rotations for all events, sometimes hidden in the noise.

In order to quantify and document the observations systematically, we focus on four earthquakes with visible P coda rotations (signal to noise ratios S/N ≥ 1.86). Their magnitudes, epicenter distances, and back azimuths are given in Table 2.

Frequency dependence of correlation

One of the expectations of ring laser measurements is to help seismologists separating P and S waves in the wave field (e.g., Takeo, 1997). The appearance of P coda rotations seems to frustrate that hope. Since the dominant periods of directly arriving energy of P and S waves are different, we investigate the cross-correlation between high-pass filtered transverse acceleration and rotation rate as a function of time and cutoff period. Sliding window lengths were taken twice as long as the cutoff periods. The cutoff period range was chosen large enough to cover at least the dominant periods of the directly arriving P - energy (around 1s) and S - energy (around 5s). Typical results are shown in Figure 5a and 5b (see also Igel et al., 2007). At the bottom subplots, the zero-lag-normalized-cross correlation coefficients as a function of time and cut-off period are presented in the same window as the seismograms. At high frequencies, we can see a sharp increase in correlation at and following the direct P – wave (subplot 4 from top and the bottom).

This correlation smears out and becomes less pronounced with increasing period, while the corresponding correlation of SH and Love wave type signals increases with period. It is interesting to note the distinct increase of correlation at specific arrival times. This may well indicate specific seismic phases (shear waves, P-S conversions).

Directional dependence of correlation

So far, the translation data were rotated into transverse and radial components according to the theoretical back-azimuth derived from known coordinates of earthquake epicenter and observation station. But – as shown in Igel et al. (2007) – the cross correlation is highly azimuth dependant. For S and Love waves it allows estimating back azimuth. In the P coda it may give hints as to where the SH energy comes from. To investigate this further the directional dependence of the correlation between horizontal acceleration and rotation rate is examined in detail.

We calculate horizontal acceleration with assumed back azimuths varying in the range of $0\text{-}360^0$ then examine the zero-lag-normalized-cross-correlation-coefficients between horizontal acceleration and rotation rate in sliding time windows. High pass filters with appropriate cut-off periods were applied before correlating. Sliding window lengths were taken twice as long as the cut-off periods. Figure 6 shows typical results for the case of the Tokachi-oki event. In the fifth subplot (from top) and the bottom of this figure, the correlation coefficients as a function of time and assumed back azimuth are shown in the same time window. In the fourth and the fifth subplots cut-off period T=5s and sliding window length 10s were used. High correlation coefficients are distributed around the theoretical back azimuth (indicated by a horizontal black line) at the onset times of SH and Love waves. When the cut-off period T=1s and sliding window length 2s were used (bottom two subplots), we observe at the bottom of this figure that high

correlation coefficients are more evenly distributed with angle in the P coda, suggesting rotational energy to come from all directions.

To estimate the back azimuth at longer periods, we sum up over time the correlation coefficients that were calculated with cut-off periods $T \geq 5s$ (dominant period of directly arriving S wave) over a window containing SH and Love waves. The estimated back azimuth is associated with the maximum of the sum. In Figure 7 the distribution of the normalized sums as a function of assumed back azimuth are shown for four typical events (Algeria 21-05-2003, M6.9; Russia 27-09-2003, M7.5; Tokachi-oki 25-09-2003, M8.1; Sumatra 12-09-2007, M8.4). For all these events, there exist clear maxima. The theoretical back azimuths indicated by horizontal black lines correspond almost exactly to the peaks of the normalized sums. The estimated and theoretical back azimuths, respectively, are 223^0 & 212^0 (Algeria event), 63^0 & 59^0 (Russia event), 38^0 & 35^0 (Tokachi-oki event), and 86^0 & 94^0 (Sumatra event). The difference can be explained by the influence of 3D structure on the propagation direction or the non-planarity of the wave fronts. This processing can be used to estimate the direction of the incoming seismic transversely polarized wave field.

To investigate the direction of the incoming energy of P coda rotations, we examine the distribution of the same normalized sums over the window of the P coda for cases with cut-off periods $T \leq 2s$ (around dominant period of directly arriving P wave). The results are shown in Figure 8. The normalized sums in the P coda have almost even distributions with angle for all four events. This result implies that energies of high frequency rotational motions about a vertical axis in the P coda come from many different directions, indicative of a strongly scattered wave field.

Envelopes

As mentioned above, tilt-ring laser coupling or scattering may contribute to the P coda rotations. If tilt-ring laser coupling strongly contributes to the observations, energies of the P coda rotations should appear right after the onset of P waves. Therefore, we investigate in the following the time-dependent variation of energies of observed translation and rotational seismograms in the P coda.

In seismology, the envelope of a time series is an unsigned low-pass of the original signal. It shows the time-dependent variation of amplitudes (or energies) of the time series. The normalization erases any influence of polarities in order to ease recognition of similarities or differences in the wave - forms. However relative amplitudes within the trace are preserved.

The normalized envelope Y of a seismogram X is defined as:

$$Y(t) = \frac{abs(X(t)) + j * H(X(t))}{\max(abs(X(t)) + j * H(X(t)))}$$

In this definition j is the imaginary unit, and H represents the Hilbert transform of time series X.

The normalized envelopes of rotation rate and the vertical and transverse components of ground velocities are calculated. The results for four earthquakes are shown in Figure 9. In each subplot (from top, respectively) individually normalized envelopes of vertical, transverse velocities, rotation rate, superposition of the envelopes of vertical and transverse velocities, and of vertical velocity and rotation rate of each event are shown. We can recognize that the amplitude of vertical velocity (the top trace) increases very fast right after the P wave onset.

Whereas, after the arrival time of the direct P wave the amplitude increase of transverse velocity and rotation rate is delayed (the second and third traces from top and the two bottom traces). However, the increases of transverse velocity and rotation rate amplitudes remain even though the amplitude of vertical velocity passes its maximum value and decreases.

Before proceeding to model aspects of these observations, we can summarize that the energies of the observed P coda rotations are predominant at high frequencies, come from many different directions, and increase with time slower than that of the direct P waves. These results suggest that P-SH scattering is the dominant cause for the observations. We proceed to quantify these observations by modeling complete six-component seismograms in 3D random media.

Modeling

Scattering is a phenomenon generated by the interaction between primary waves and inhomogeneities. In this process the amplitudes of the primary seismic waves are reduced as they propagate, but the energy of the propagating wave field is conserved. As mentioned by Stein and Wysession (2003), this process can be described by elastic wave theory in which the governing parameters are: (1) the wavelength of the wave field (or the wave number); (2) the distance that the wave travels through the heterogeneous region; (3) the heterogeneity size; and (4) the velocity perturbation. When the size of the velocity heterogeneities is close to the wavelength of the wave field and the travel distance is large enough compared to the wavelength, scattered energy is predominant (Stein and Wysession, 2003; Aki and Richards, 1980, 2002). Random media can be generated for desired correlation lengths and velocity perturbations (e.g., Klimeš, 2002).

The purpose of the forward modeling in this section is to study the generation of P coda rotations under the assumption of P-SH scattering in the crust. Thus, any other contribution to the P coda rotations except P-SH scattering needs to be avoided. To satisfy this, we model complete theoretical seismograms created by a plane P wave of dominant period 1s (the same as the predominant period of the observed P waves), propagating upward in vertical direction from the bottom of a random medium.

A random medium can be described through a spatial distribution $u(x)$ of material parameters u. This distribution can be expressed as (Klimeš, 2002):

$$u(x) = u_0(x) + U(x)$$

where $u_0(x)$ is the mean value of $u(x)$ and $U(x)$ is a realization of the random quantity. In our study, to simplify the modeling, we perform simulations with random media in which the wave velocities are randomly perturbed in space, but the mass density ρ, the ratio between P and S wave velocities V_p/V_s, and the mean values of the velocities are kept constant. The realization of the random velocities is calculated in terms of white noise filtered by a spectral filter (see Klimeš, 2002). Since we just consider high frequencies (i.e., small heterogeneities), we choose the spectral filter corresponding to the high-pass filtered Zero Von Kármán random medium mentioned in Klimeš (2002).

To be as realistic as possible, the used model setup is based on the crust model of Bassin et al. (2000) at the Wettzell area. The model is 60800m long, 60800m wide and 40850m deep. The mass density is taken ρ=2.9 g/cm^3, and the mean values of P and S wave velocities (respectively) are V_p= 6600m/s, V_s= 3700m/s. In order to produce significant scattering energy,

we use correlation lengths between 1000m and 15000m (see Aki and Richards, 1980, 2002; Stein and Wysession, 2003). Furthermore, the root mean square perturbation of wave velocities is taken in the range from 0% (homogeneity) up to about 11%.

Seismograms are calculated using the ADER-DG method (the combination of a Discontinuous Galerkin finite element method and an Arbitrary high-order DERivative time integration approach developed by Dumbser and Käser, 2006) that was extended to allow outputting the three components of rotation rate, in addition to the three components of translational velocity. The modeling parameters are detailed in Table 3.

Figure 10 illustrates schematically a three-dimensional Von Kármán random medium used in this study with correlation length a = 2000m, root-mean square perturbation of 6.51%. In addition, synthetic seismograms obtained at three receivers located at different sites on the surface of the model are shown. For each set of translational velocities (V_x, V_y, V_z) or rotation rates (Ω_x, Ω_y, Ω_z) the amplitudes are scaled. The figure shows that, as waves travel through the random medium, both rotational and horizontal translation components are generated by scattering. The delayed arrival of the vertical rotation compared to the onset of the vertical velocity that we noticed in the observations can also be clearly seen in our synthetics. Moreover, the simulated seismograms differ at each station because the random field is completely three-dimensional. This allows us to stack aspects of the data from different receivers rather than multiple simulations.

To investigate systematically the effects of the perturbation on P coda rotations, we first fix the correlation length to 2000m then calculate seismograms with different velocity perturbation amplitudes. Figure 11 shows the simulated seismograms obtained at the receiver located at the center of the model surface as a function of time and velocity perturbation. We can

see that for a homogeneous medium (i.e., zero perturbation) no rotational or horizontal translations are generated. Energy in these components appears only in the case of random media. We can also observe that, as the velocity perturbation increases, the peak amplitudes of these signals increase, while the vertical velocity decreases.

The effects of the scattering can be quantified by considering both the peak amplitudes and energy of all six components of motion at the surface. The energy, defined as the sum over the squared amplitude, will be referred to as simply as "energy" in the following. More information on the concept of elastic wave energy density can be found in Hennino et al. (2001). Furthermore, since the media are random in all three dimensions, we perform an average of the peak amplitudes and energies computed at 24 receivers located around a circle of a radius 15000m on the surface of the model (see Figure 10), taking the first 21s of each trace. In total we investigate 10 different random models characterized by varying velocity perturbations.

The results shown in Figure 12 imply that part of the energy in the vertical component is scattered into energy of rotational and horizontal motions. This figure suggests that the ratio of energies of rotation rate and vertical velocity can be used to characterize and eventually constrain scattering. Another result illustrated in Figure 12 is that the horizontal components of rotation rate (i.e. tilt) have generally higher amplitudes than the vertical ones.

The key question is: how can we compare the simulated P coda rotation with the observed ones? We follow studies by Shapiro et al. (2000) and Hennino et al. (2001) who proposed using the ratio of energies of curl and divergence of ground motions to distinguish between the different scattering regimes in the lithosphere. Using the curl of the wave field derived from array-translation measurements, the authors showed that there is an energy equipartition, indicated by the stabilization of the energy ratio.

We first return to the observations and investigate the ratio of energies (i.e. sum of squared amplitudes) of observed rotation rate (Ω_z) and vertical velocity (V_z) in sliding time windows from the onset of P waves along the P coda. The length of the sliding time windows was varied from 5s to 20s. Figure 13a shows a typical result for the case of the Sumatra earthquake 12-09-2007, M8.4. We observe that after the P arrival, the ratio is reduced (the third trace from top, before 810s). After a short time of decrease, the energy ratio is quite stable until the energy of V_z reaches the maximum value (section between 810s and 860s). Then the energy ratio starts increasing because the amplitude of V_z is decreased while that of Ω_z is still increasing (section between 860s and 965s). The ratio reaches the peak value when the energy of Ω_z in the sliding time window reaches the maximum value. Zooming in the ratio in the section between 800s and 875s (bottom) we can see that for cases of window lengths 15s and 20s the ratios have a stable value of about $1x10^{-8}$. For smaller window lengths (5s, 10s) the ratios vary around this value. For the case of the Tokachi-oki earthquake 25-09-2003, M8.1 we obtain the same result with the stable value of the energy ratio being about $1.8x10^{-8}$ (Figure 13b, bottom, section between about 7340s and 7365s).

These ratios are calculated for windows of varying duration beginning at the onset of P wave. The results for four typical events are shown in Figure 14 with the lengths of the windows given by the horizontal axis. The figure shows that after the window length reaches 15s the energy ratios for different events attain a quite stable value of about $1.1\text{-}2.6x10^{-8}$, almost the same value that we obtained with sliding windows before. This stable value remains in a range of window length from 15s to 35s for all four events (bottom). We return to the modeling part to investigate which scattering parameters are compatible with the observed energy ratio.

We use a window of 15s length beginning at the onset of the P wave synthetics. For each pair of scattering parameters (a velocity perturbation and a correlation length), we obtain a value of the energy ratio, averaged through all 24 receivers in circular configuration (Figure 10). Initially, we take a fixed correlation length of 2000m and calculate the average energy ratios as a function of velocity perturbation. The results are shown as a black line in Figure 15. As expected, the energy ratio increases as we increase the perturbation. The curve shows a non-linear behavior, with the slope decreasing as the perturbation increases. Similarly, we can calculate the average energy ratio as a function of correlation length at some fixed values of velocity perturbation. We cover a range of correlation lengths from 1000m up to 15000m and fixed perturbation values of 4.8%, 6.1% and 8%. The results are plotted as squares in Figure 15 and strongly suggest that for our model geometry the energy ratio is much more sensitive to the velocity perturbation than to the correlation length.

We can finally try to explain the origin of the $1.1\text{-}2.6\text{x}10^{8}$ value for the energy ratio consistently observed at Wettzell. Although the value of the correlation length, i.e., the size of the scatterers, cannot be constrained, our simulations show that the observed range of energy ratios (as can be seen in the grey area of Figure 15) are compatible with crust models containing velocity perturbation values ranging from 4.8% to 6.5%.

Discussions and conclusions

The first observations of the ring laser rotational signals in the P coda of tele-seismic events were reported by Igel et al. (2007). However, the origin of the P-coda-rotations was

unclear. The main goals of this study are (1) to characterize the observations of P coda rotations in detail, and (2) to model the observations in terms of P-SH scattering.

The observations presented in this paper indicate that the energies of the P coda rotations are predominant at high frequencies, come from many different directions, and increase in time slower than that of the energy in the vertical component of translation. The distribution of cross-correlation coefficients between rotation rate and transverse acceleration as a function of time and cut-off period demonstrates an effective tool to separate direct S waves from the scattering field. The explanation for the P coda rotations by P-SH scattering is affirmed by the simulation results shown in this study. Under the assumption of a random crustal medium, rotational signals in the P coda can be generated efficiently.

The phenomenon of energy equipartitioning into P and S waves studied by Shapiro et al. (2000) and Hennino et al. (2001) is considered as the principle of multiple scattering. Our study provides further evidence of energy equipartition, indicated by the stabilization of the ratio of energies of vertical rotation rate and vertical translation velocity after the onset of P wave. This stable energy ratio allows us to constrain the velocity perturbation of the random crustal model. Under the assumption of a Von Kármán random medium, we obtain velocity perturbation values ranging from 4.8% to 6.5% for the Wettzell area.

In summary, it can be concluded that P-SH scattering in the crust can explain the P coda observations and rotation sensors offers a direct measurement of SH energy and thus may help understanding the partitioning of P and S energy. The contributions of anisotropy, topography scattering in the observed P coda rotations remain open issues and will be addressed in the future.

Data and Resources

The observed seismograms of period 2003-2004 used in this study were provided by Geophysics Section, Ludwig Maximilians University Munich and published by Igel et al., 2007. The seismograms of events occurred after September of 2007 can be obtained from the WebDC - Integrated Seismological Data Portal at http://www.webdc.eu/arclink/query?sesskey=0841ed49.

Acknowledgments

The research was supported by the Geophysics Section - LMU Munich, the Vietnamese Government (Project 322), and the German Academic Exchange Service (DAAD). We acknowledge the contributions of the Bundesamt für Kartographie und Geodäsie (BKG) towards the installation and operation of the 'G' ring laser at the geodetic observatory Wettzell. We are grateful to František Gallovič for providing the code to create random media. Thanks to Michael Campillo, Christoph Sens-Schönfelder and Nicolai Shapiro for comments.

References

Aki, K. & Richards, P. G. *Quantitative Seismology*, 2nd Edition, University Science Books (2002).

Bassin, C., Laske, G. and Masters, G., The Current Limits of Resolution for Surface Wave Tomography in North America, *EOS Trans AGU*, 81, F897, 2000.

Cochard, A., Igel, H., Schuberth, B., Suryanto, W., Velikoseltsev, A., Schreiber, U., Wassermann, J., Scherbaum, F., Vollmer, D. Rotational motions in seismology: theory,

observations, simulation, in "*Earthquake source asymmetry, structural media and rotation effects*" eds. Teisseyre et al., Springer Verlag (2006).

Dumbser, M., and M. Käser. An Arbitrary High Order Discontinuous Galerkin Method for Elastic Waves on Unstructured Meshes II: The Three-Dimensional Isotropic Case, *Geophysical Journal International*, *167*(1), 319-336, doi:10.1111/j.1365-246X.2006.03120.x. (2006).

Fichtner A. and Igel H., Sensitivity densities for rotational ground motion measurements - A new imaging tool for crustal structures!, Bull. Seism. Soc. Amer., this issue, (2008).

Graizer, V. M. Effect of tilt on strong motion data processing, Soil Dyn. Earthq. Eng, 25, 197-204 (2005).

Graizer, V. M. Equation of pendulum motion including rotations and its implications to the strong-ground motion, in Earthquake Source Asymmetry, Structural Media and Rotation Effects, 471-491 (2006).

Hennino R., Trégourès N., Shapiro N. M., Margerin L., Campillo M., van Tiggelen B. A., and Weaver R. L. Observation of Equipartition of Seismic Waves, *Physical Review Letters*, 86, 3447-3450,doi: 10.1103/PhysRevLett.86.3447 (2001).

Igel, H., Cochard, A., Wassermann, J., Flaws, A., Schreiber, U., Velikoseltsev, A., Pham, D.N. Broadband Observations of Earthquake Induced Rotational Ground Motions, *Geophys. J. Int.*, 168, 182-196, doi: 10.1111/j.1365-246X.2006.03146x (2007).

Igel, H., Schreiber, K.U., Flaws, A., Schuberth, B., Velikoseltsev, A., Cochard, A. Rotational motions induced by the M8.1 Tokachi-oki earthquake, September 25, 2003, *Geophys. Res. Lett.*, 32, L08309, doi:10.1029/2004GL022336 (2005).

Klimeš L. Correlation functions of random media, *Pure appl. geophys.*, 159, 1811-1831 (2002).

Li, H., Sun, L., Wang, S. Improved Approach for Obtaining Rotational Components of Seismic Motion. *Transactions*, SmiRT 16, 1-8 (2001).

Li, H., Sun, L., Wang, S. Frequency dispersion characteristics of phase velocities in surface wave for rotational components of seismic motion. *Journal of Sound and Vibration*, 258 (5), 815-827 (2002).

McLeod, D.P., Stedman, G.E., Webb, T.H. & Schreiber, U. Comparison of standard and ring laser rotational seismograms. *Bull. Seism. Soc. Amer.* 88, 1495-1503 (1998).

Pancha, A., Webb, T.H., Stedman, G.E., McLeod, D.P. & Schreiber, U. Ring laser detection of rotations from teleseismic waves. *Geophys. Res. Lett*. 27, 3553-3556 (2000).

Pham D.N., Igel H., Wassermann, J., Cochard, A., Schreiber, U. Cross-axis sensitivity of optical rotation sensors, Bull. Seism. Soc. Amer., this issue, (2008).

Pillet R. and Virieux J. The effects of seismic rotations on inertial sensors, *Geophys. J. Int.*, doi: 10.1111/j.1365-246X.2007.03617.x (2007).

Schreiber, U., Igel, H., Cochard, A., Velikoseltsev, A., Flaws, A., Schuberth, B., Drewitz, W., Müller, F., The GEOsensor project: A new observable for seismology. In "Observation of the System Earth from Space", Springer (2005).

Schreiber, U., Stedman, G.E., Igel, H., Flaws, A. Ring laser gyroscopes as rotation sensors for seismic wave studies. In "*Earthquake source asymmetry, structural media and rotation effects*" eds. Teisseyre et al., Springer Verlag (2006).

Shapiro N. M., Campillo M., Margerin L., Singh S. K., Kostoglodov V., and Pacheco J. The Energy Partitioning and the Diffusive Character of the Seismic Coda, *Bull. Seism. Soc. Am.,* 90, 655–665, (2000).

Stein S. and Wysession M. An Introduction to Seismology, Earthquake, and Earth Structure, Blackwell Publishing (2003).

Takeo, M. & Ito, H.M. What can be learned from rotational motions excited by earthquakes? *Geophys. J. Int.* 129, 319-329 (1997).

Takeo, M. Ground rotational motions recorded in near-source region of earthquakes. *Geophys. Res. Lett*. 25, 789-792 (1998).

Trifunac, M.D. & Todorovska, M.I. A note on the usable dynamic range of accelerographs recording translation. *Soil Dyn. and Earth. Eng*. 21(4), 275-286 (2001).

Authors affiliations, addresses

Nguyen Dinh Pham[*], Heiner Igel, Joachim Wassermann, Martin Käser, Josep de la Puente

Geophysics Section,

Department of Earth and Environmental Sciences,

Ludwig Maximilians Universität München,

Theresienstrasse 41,

80333 München, GERMANY.

Ulrich Schreiber

Forschungseinrichtung Satellitengeodäsie,

Technical University Munich,

Fundamentalstation Wettzell, Sackenriederstrasse 25,

D-93444 *Kötzting, GERMANY.*

(*) Institute of Geophysics,

Vietnamese Academy of Science and Technology,

18 Hoang Quoc Viet, Cau Giay, Hanoi, VIETNAM.

Tables

Table 1. Earthquakes used in this study

Date (yy, mm, dd)	Mag. (L,b,S, W)	Lat. (deg.)	Long. (deg.)	Depth (km)	Region	Distance (km)	Baz (deg.)	Note for rot. rate in the P coda
03/05/21	6.9	36.96	3.63	12	Algeria	1547.2	212.3	Visible
03/05/26	7.0	38.85	141.57	68	Honshu	9009.2	38.0	Visible
03/07/06	5.7	40.44	26.02	17	Turkey	1415.1	128.2	Invisible
03/08/14	6.3	39.16	20.60	10	Greece	1268.6	148.2	Visible
03/09/25	8.1	41.80	143.91	27	Tokachi-oki	8828.0	34.9	Visible
03/09/27	7.5	50.04	87.81	16	Russia	5164.8	58.8	Visible
03/09/27	6.6	50.09	87.76	10	Russia	5158.9	58.8	Invisible
03/10/01	7.1	50.21	87.72	10	Siberia	5149.9	58.7	Invisible
03/10/08	6.7	42.65	144.57	32	Hokkaido	8773.3	34.0	Invisible
03/10/31	7.0	37.81	142.62	10	Honshu	9155.4	37.8	Invisible
03/11/17	7.8	51.15	178.65	33	Rat Islands	8780.6	9.0	Invisible
03/12/26	6.8	29.00	58.31	10	Iran	4426.5	103.3	Invisible
04/02/05	7.1	-3.62	135.54	16	Irian-Jaya	12629.5	66.5	Invisible
04/02/07	7.5	-4.00	135.02	10	Irian-Jaya	12628.5	67.2	Invisible
04/02/24	6.3	35.20	-4.00	0	Al Hoceima	2074.0	227.9	Invisible
04/03/17	6.1	34.59	23.33	24	Greece	1831.7	148.2	Invisible
04/04/05	6.6	36.51	71.03	187	Afghanistan	4817.6	84.3	Invisible
04/05/28	6.4	36.29	51.61	17	Iran	3424.5	100.0	Invisible
04/05/29	6.6	34.25	141.41	16	Honshu	9440.2	40.5	Invisible
04/12/05	5.0	48.12	8.08	10	Germany	370.8	253.8	Visible
04/12/26	9.3	3.30	95.98	30	Sumatra	9228.4	93.1	Visible
07/09/12	8.4	-4.44	101.37	34	Sumatra	10271.0	94.0	Visible
07/10/31	6.5	51.37	-178.38	28	Mariana Isl.	8787.0	352.9	Visible
07/11/14	7.6	-22.23	-69.91	40	North Chile	11356.0	249.9	Visible
07/12/09	7.2	-26.06	-177.52	190	South Fiji	17296.0	336.9	Visible
07/12/19	7.0	51.50	-179.50	60	Alentia	8763.0	352.2	Invisible
08/01/06	6.5	37.40	22.70	70	South Greece	1526.0	145.2	Visible
08/01/09	6.3	32.70	85.20	50	Xizang	6098.6	78.7	Invisible
08/02/08	6.1	11.00	-42.70	10	Atlantic	6617.8	250.0	Visible
08/02/14	7.0	36.60	21.70	30	Greece	1566.7	149.6	Visible
08/02/14	6.1	36.50	21.90	33	Greece	1584.2	149.2	Visible
08/02/19	5.1	36.40	21.80	40	Greece	1590.6	149.7	Invisible
08/02/20	7.6	2.90	96.00	33	Sumatra	9263.6	93.3	Invisible

08/02/20	6.2	36.50	21.70	25	Greece	1576.8	149.8	Visible
08/02/21	6.1	77.10	18.40	10	Svalbard	3117.7	2.6	Invisible
08/02/25	7.3	-2.50	99.90	33	Sumatra	10001.0	93.9	Invisible

Table 2. Earthquakes studied in detail

Date (yy, mm, dd)	Mag. (L,b,S, W)	Lat. (deg.)	Long. (deg.)	Depth (km)	Region	Distance (km)	Baz (deg.)	S/N (P coda)	
								Vz	Rz
03/05/21	6.9	36.96	3.63	12	Algeria	1547.2	212.3	158.18	2.53
03/09/25	8.1	41.80	143.91	27	Tokachi-oki	8828.0	34.9	359.82	2.75
03/09/27	7.5	50.04	87.81	16	Russia	5164.8	58.8	143.24	1.86
07/09/12	8.4	-4.44	101.37	34	Sumatra	10271.0	94.0	58.60	2.93

Table 3. The modeling parameters used in this study

Mesh type	Hexahedral
Element edge length	950m
Total number of elements	176128
Polynomial order inside elements	4
Number of processors	64
Length of seismograms	60s
Boundary conditions	Free surface (top), inflow (bottom), periodic (sides)
Average time step	8.13008×10^{-3}s
Run time per simulation	~ 2 hours

Figure Captions

Figure 1. Magnitude distribution of the observed events as a function of epicenter distance.

Figure 2. Observations of translation and rotational ground motions induced by the Sumatra earthquake 12-09-2007, M8.4. Top three traces: Unfiltered vertical and transverse components of ground acceleration and rotation rate (respectively). Bottom three traces: low-pass filtered rotation rate with cut-off periods 1s, 5s, and 10s (respectively). Significant energy of rotational motions in the P coda is visible and predominant at high frequencies.

Figure 3. Top three traces: Vertical, transverse accelerations and rotation rate (respectively) for the Al Hoceima event 24-02-2004, M6.4. Bottom: zero-lag normalized cross-correlation coefficients between rotation rate and transverse acceleration calculated for 2s sliding time windows (after high-pass filtering with cut-off period 1s).

Figure 4. Zero-lag normalized cross-correlation coefficients between rotation rate and transverse acceleration in 2s sliding time windows (after high-pass filtering with cut-off period 1s) calculated for 21 events observed in 2003-2004. The correlation coefficients increase at and following the onset of P waves in all these observed events.

Figure 5a. Top three traces: Vertical, transverse accelerations and rotation rate (respectively) for the Tokachi-oki event 25-09-2003, M8.1. The fourth trace (from top): zero lag normalized cross correlation coefficients between rotation rate and transverse acceleration after high-pass filtering with cut-off period 1s, calculated for 2s sliding time

windows. Bottom: the correlation coefficients as a function of time and cut-off period (length of sliding time window is twice as long as the high pass cut off period).

Figure 5b. (Continued.) Top three traces: Vertical, transverse accelerations and rotation rate (respectively) for the Sumatra event 12-09-2007, M8.4. The fourth trace (from top): zero lag normalized cross correlation coefficients between rotation rate and transverse acceleration after high-pass filtering with cut-off period 1s, calculated for 2s sliding time windows. Bottom: the correlation coefficients as a function of time and cut-off period (length of sliding time window is twice as long as the high pass cut off period).

Figure 6. Top three traces: Vertical, transverse accelerations and rotation rate, respectively, for the Tokachi-oki event 25-09-2003, M8.1. The fourth and sixth traces (from top): zero lag normalized cross-correlation coefficients between rotation rate and transverse acceleration after high-pass filtering with cut-off periods 5s and 1s, calculated for 10s and 2s sliding time windows (respectively). The fifth and bottom: the correlation coefficients as a function of time and assumed back-azimuth (high pass filter with cut off period 5s and 1s, sliding time windows of 10s and 2s were applied respectively). The theoretical back-azimuth is indicated by a horizontal line.

Figure 7. Distribution of the (normalized) sum of the correlation coefficients (between rotation rate and transverse acceleration after high-pass filtering with cut-off period 5s, 8s and 10s, length of sliding time window are twice as long as the cut off period applied before correlating) in the window containing direct SH and Love waves of several observed events as a function of assumed back azimuth.

Figure 8. Distribution of the (normalized) sum of the correlation coefficients (between rotation rate and transverse acceleration after high-pass filtering with cut-off period 1s, 1.5s and 2s, length of sliding time window are twice as long as the cut off period applied before correlating) in the P coda window of several observed events as a function of back azimuth. The almost even distribution implies that high frequency rotational energy in the P coda comes from all azimuthal directions.

Figure 9. Normalized envelopes of individual seismograms and their superposition. For each subplot (from top, respectively): normalized envelopes of vertical and transverse components of ground velocity, vertical component of rotation rate, and the superposition of the envelopes of vertical and transverse velocities, and of vertical velocity and rotation rate.

Figure 10. Schematic illustration of a 3D Von Kármán random medium used in this study (correlation length a = 2000m, root-mean square perturbation of V_S is 6.51%) and 6-component-seismograms obtained at three different receivers for a plane P wave propagating upward (in a vertical direction) from the bottom of the model. For each set of translational velocities (V_x, V_y, V_z) or rotation rates (Ω_x, Ω_y, Ω_z) amplitudes are scaled.

Figure 11. Variations of 6-component-seismograms obtained at one receiver as a function of velocity perturbation of the random medium (correlation length is fixed at 2000m) when a plane P wave propagates upward (in vertical direction) from the bottom of the model.

Figure 12. Variations of (the average values of) energy and peak amplitude of each translation and rotation component (calculated from 21s seismograms of 24 receivers distributed regularly around a circle of radius 15km from the center point at the surface of the model

– figure 10) as a function of velocity perturbation of the random medium (correlation length is fixed to 2000m) when a plane P wave propagates upward (in vertical direction) from the bottom of the model.

Figure 13a. Two top traces: Vertical components of velocity and rotation rate (respectively) in the P coda of the Sumatra event 12-09-2007, M8.4 after band-pass filtering between 0.5s and 1.5s. Two bottom traces: Ratio between energy of rotation rate and energy of vertical velocity calculated for time windows (illustrated by the vertical gray bands in the top traces) of different lengths, starting from the onset of P and sliding along the time series up to the end of the P coda.

Figure 13b. Two top traces: Vertical components of velocity and rotation rate (respectively) in the P coda of the Tokachi-oki event 25-09-2003, M8.1 after band-pass filtering between 0.5s and 1.5s. Two bottom traces: Ratio between energy of rotation rate and energy of vertical velocity calculated for time windows (illustrated by the vertical gray bands in the top two traces) of different lengths, starting from the onset of P and sliding along the time series up to the end of the P coda.

Figure 14. Ratios between energy of rotation rate and energy of vertical velocity in typical events calculated for different time windows. All the time windows start at the onset of direct P waves and their lengths are given by the horizontal axis.

Figure 15. Comparison of observed and simulated energy ratios. Black curve: the (average) energy ratio as a function of velocity perturbation calculated from simulated seismograms (correlation length fixed at 2000m); Squares: the (average) energy ratio as a function of

correlation length (from 1000m up to 15000m) obtained from simulations; Horizontal gray band: range of the energy ratios obtained from observations.

Figures

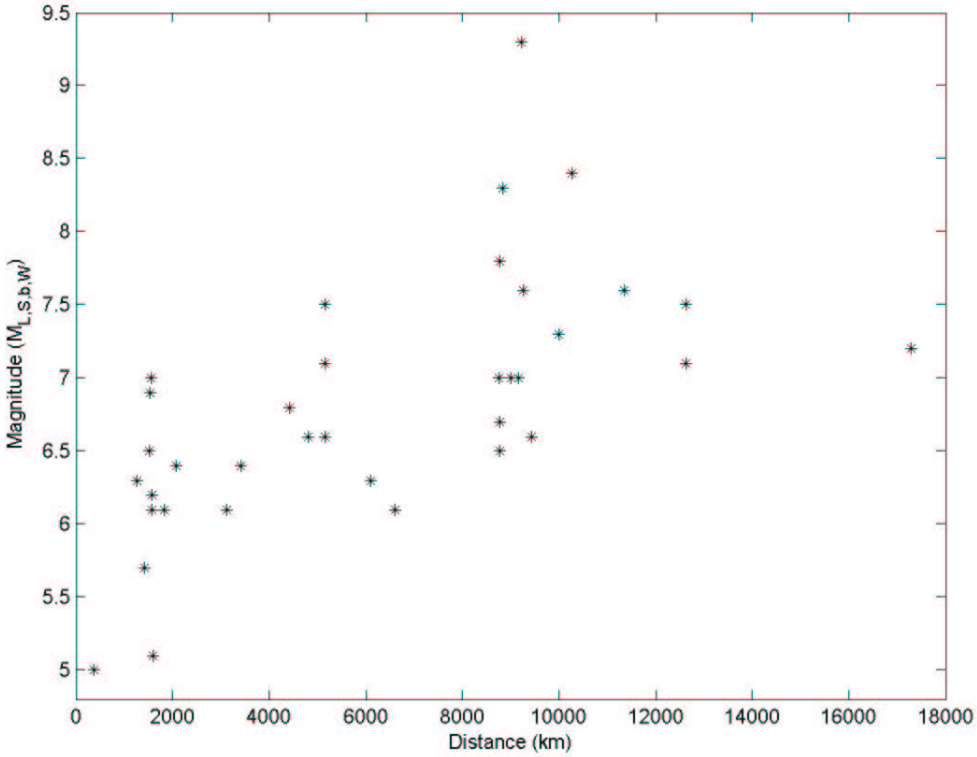

Figure 1. Magnitude distribution of the observed events as a function of epicenter distance.

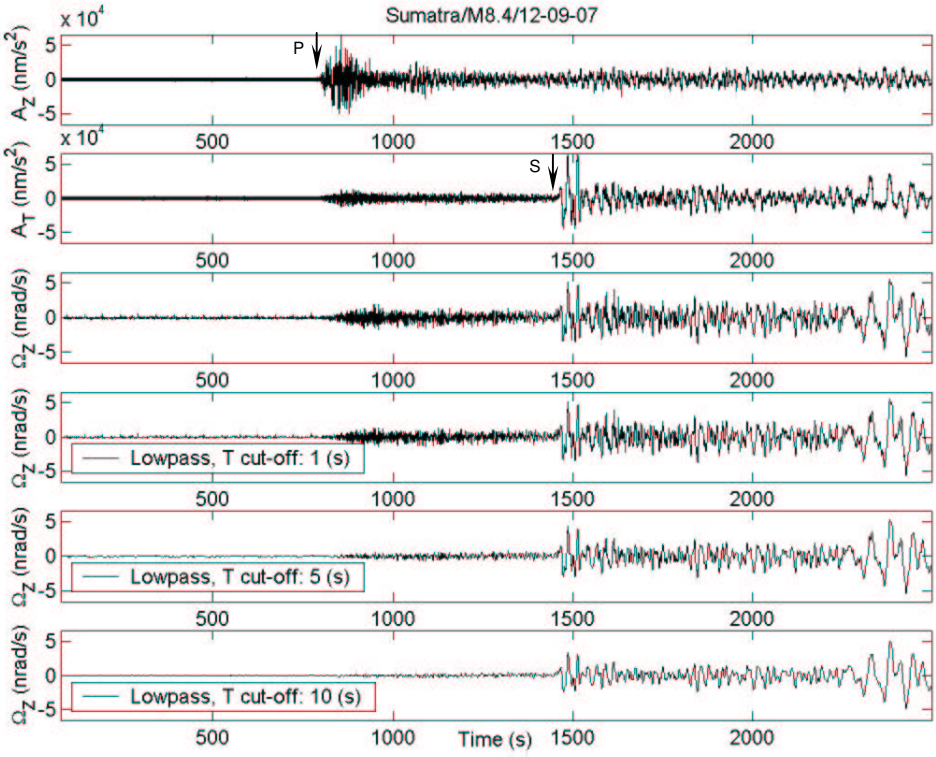

Figure 2. Observations of translation and rotational ground motions induced by the Sumatra earthquake 12-09-2007, M8.4. Top three traces: Unfiltered vertical and transverse components of ground acceleration and rotation rate (respectively). Bottom three traces: low-pass filtered rotation rate with cut-off periods 1s, 5s, and 10s (respectively). Significant energy of rotational motions in the P coda is visible and predominant at high frequencies.

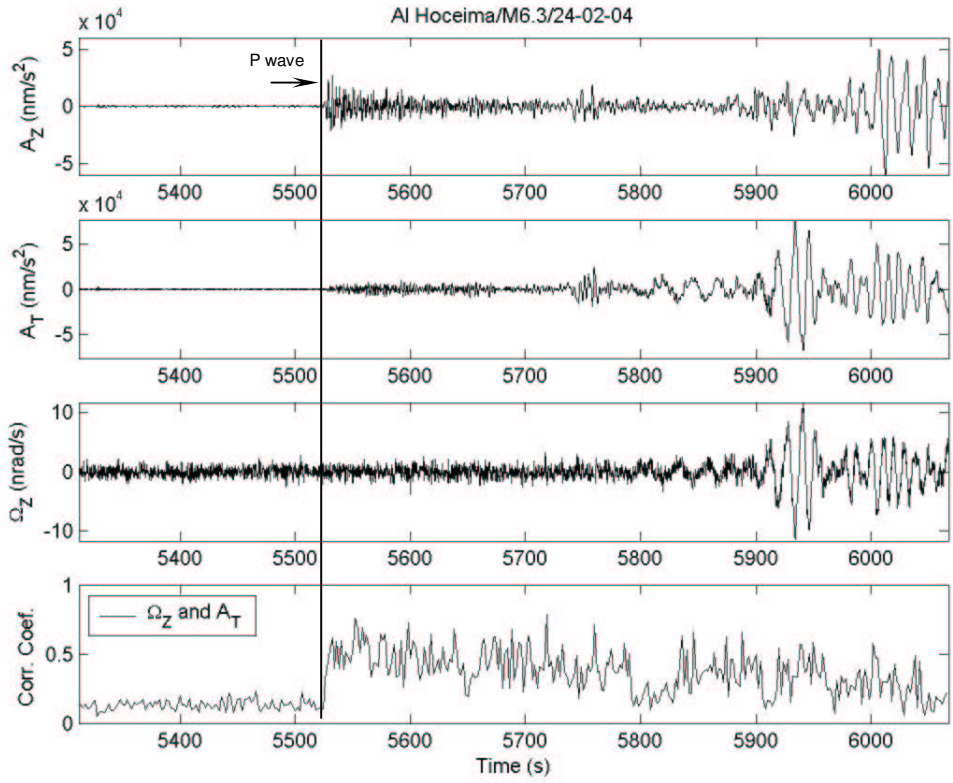

Figure 3. Top three traces: Vertical, transverse accelerations and rotation rate (respectively) for the Al Hoceima event 24-02-2004, M6.4. Bottom: zero-lag normalized cross-correlation coefficients between rotation rate and transverse acceleration calculated for 2s sliding time windows (after high-pass filtering with cut-off period 1s).

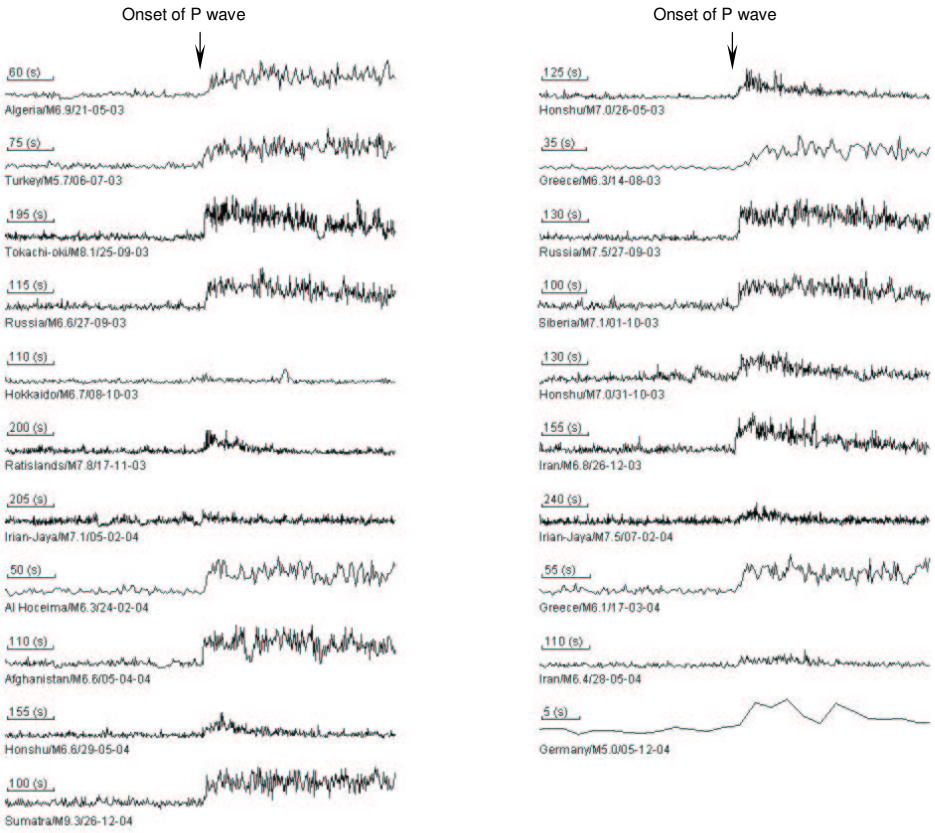

Figure 4. Zero-lag normalized cross-correlation coefficients between rotation rate and transverse acceleration in 2s sliding time windows (after high-pass filtering with cut-off period 1s) calculated for 21 events observed in 2003-2004. The correlation coefficients increase at and following the onset of P waves in all these observed events.

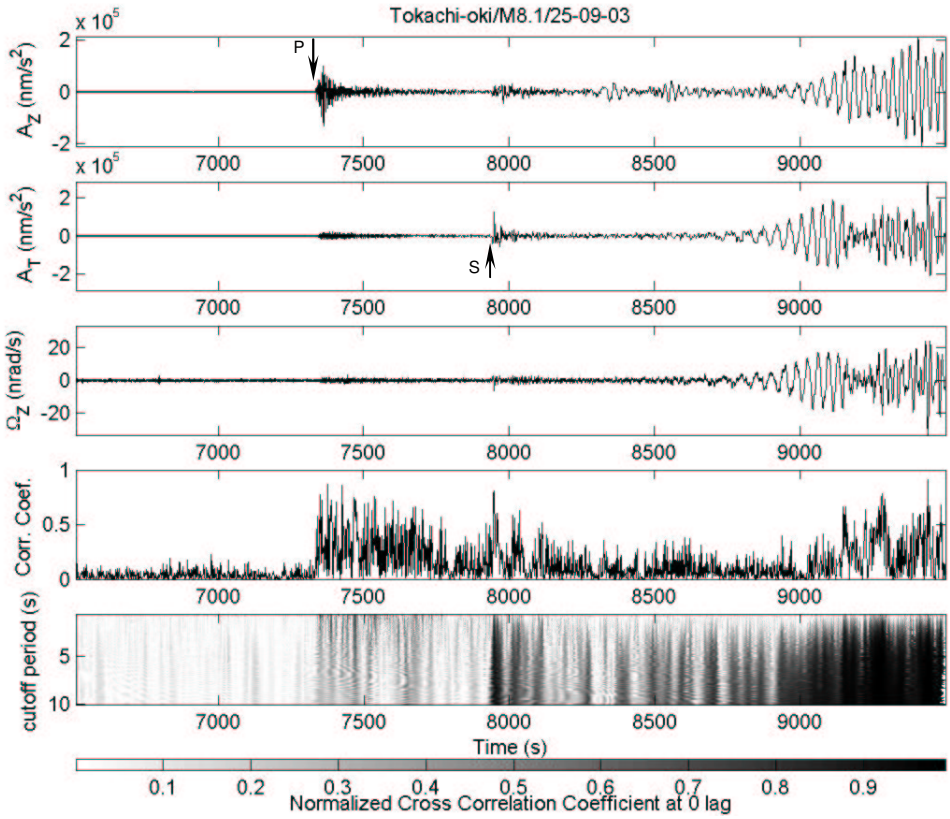

Figure 5a. Top three traces: Vertical, transverse accelerations and rotation rate (respectively) for the Tokachi-oki event 25-09-2003, M8.1. The fourth trace (from top): zero lag normalized cross correlation coefficients between rotation rate and transverse acceleration after high-pass filtering with cut-off period 1s, calculated for 2s sliding time windows. Bottom: the correlation coefficients as a function of time and cut-off period (length of sliding time window is twice as long as the high pass cut off period).

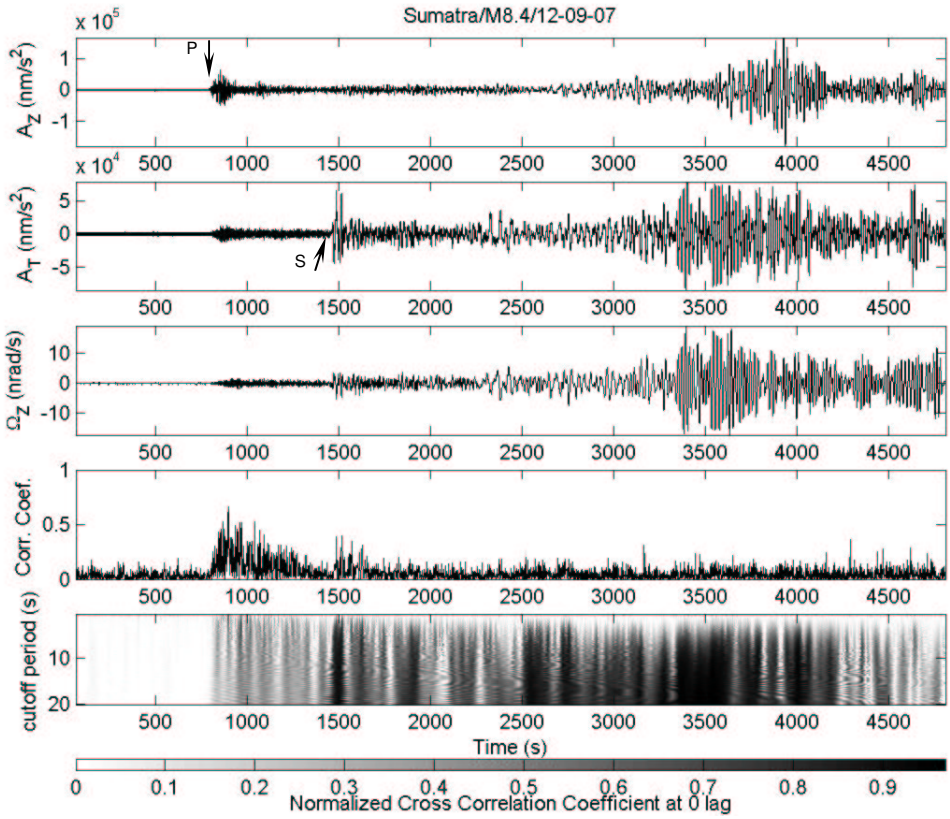

Figure 5b. (Continued.) Top three traces: Vertical, transverse accelerations and rotation rate (respectively) for the Sumatra event 12-09-2007, M8.4. The fourth trace (from top): zero lag normalized cross correlation coefficients between rotation rate and transverse acceleration after high-pass filtering with cut-off period 1s, calculated for 2s sliding time windows. Bottom: the correlation coefficients as a function of time and cut-off period (length of sliding time window is twice as long as the high pass cut off period).

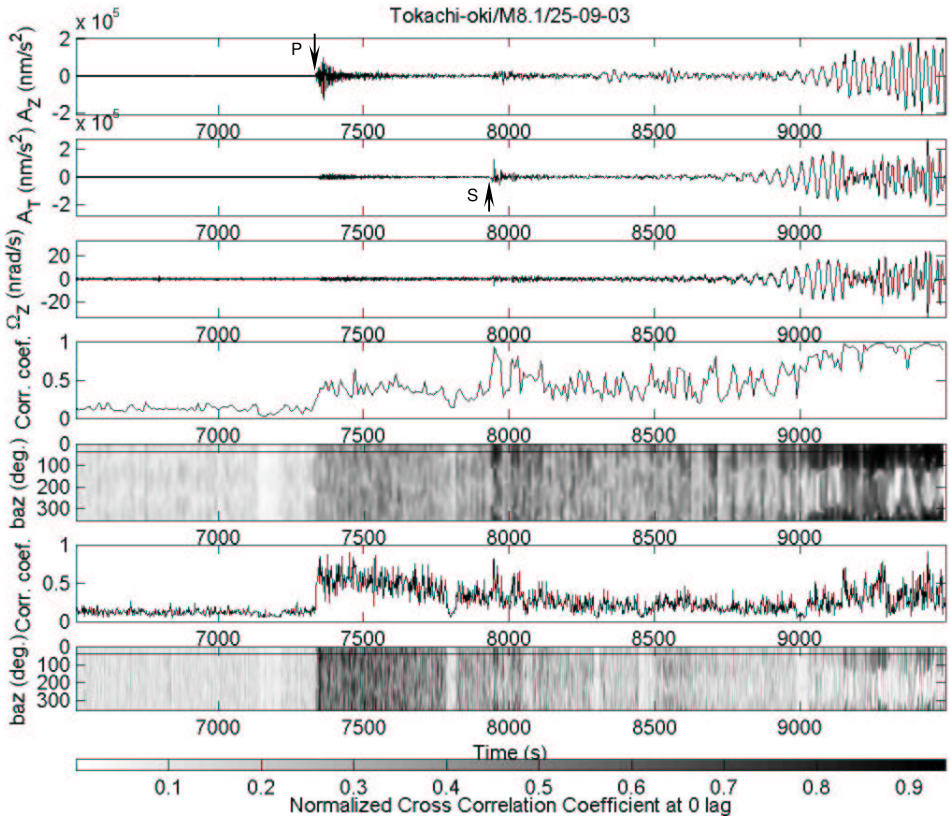

Figure 6. Top three traces: Vertical, transverse accelerations and rotation rate, respectively, for the Tokachi-oki event 25-09-2003, M8.1. The fourth and sixth traces (from top): zero lag normalized cross-correlation coefficients between rotation rate and transverse acceleration after high-pass filtering with cut-off periods 5s and 1s, calculated for 10s and 2s sliding time windows (respectively). The fifth and bottom: the correlation coefficients as a function of time and assumed back-azimuth (high pass filter with cut off period 5s and 1s, sliding time windows of 10s and 2s were applied respectively). The theoretical back-azimuth is indicated by a horizontal line.

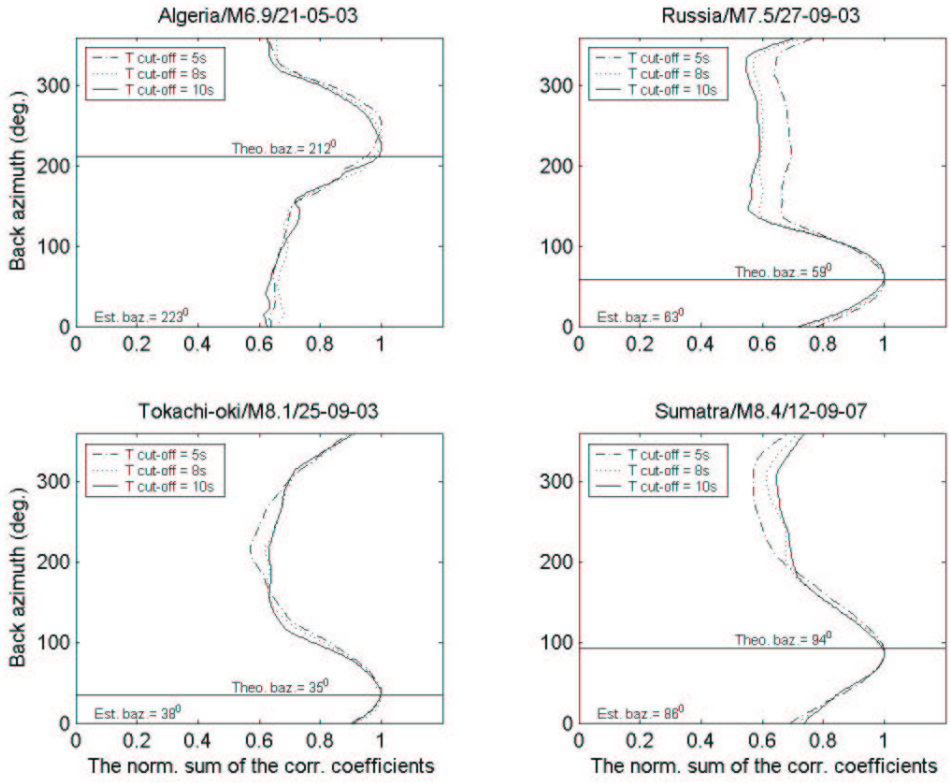

Figure 7. Distribution of the (normalized) sum of the correlation coefficients (between rotation rate and transverse acceleration after high-pass filtering with cut-off period 5s, 8s and 10s, length of sliding time window are twice as long as the cut off period applied before correlating) in the window containing direct SH and Love waves of several observed events as a function of assumed back azimuth.

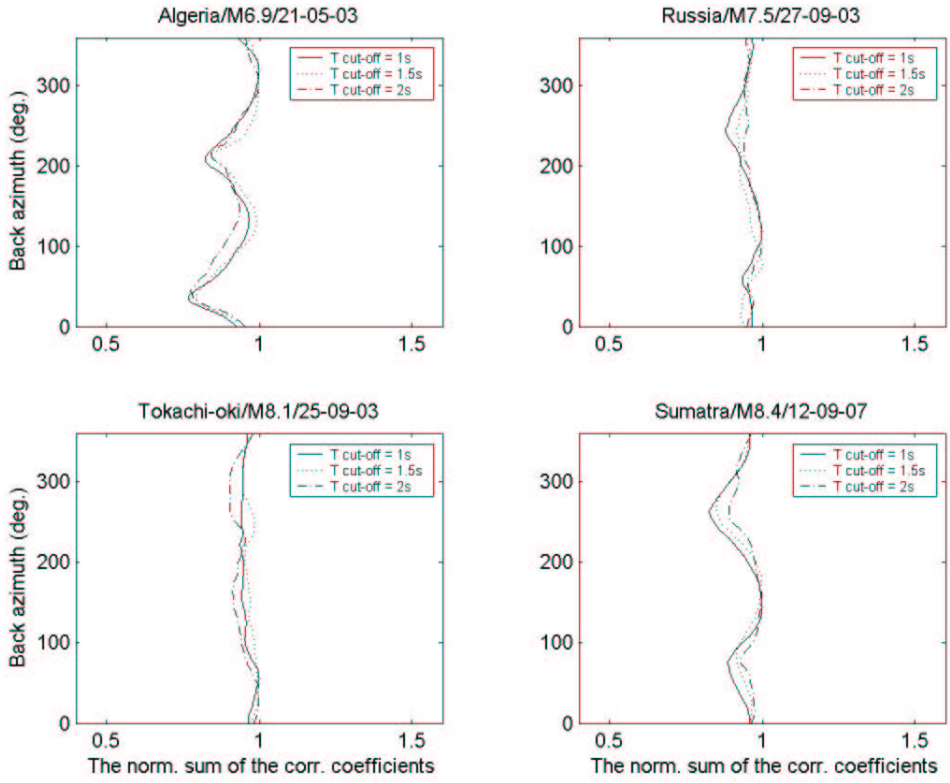

Figure 8. Distribution of the (normalized) sum of the correlation coefficients (between rotation rate and transverse acceleration after high-pass filtering with cut-off period 1s, 1.5s and 2s, length of sliding time window are twice as long as the cut off period applied before correlating) in the P coda window of several observed events as a function of back azimuth. The almost even distribution implies that high frequency rotational energy in the P coda comes from all azimuthal directions.

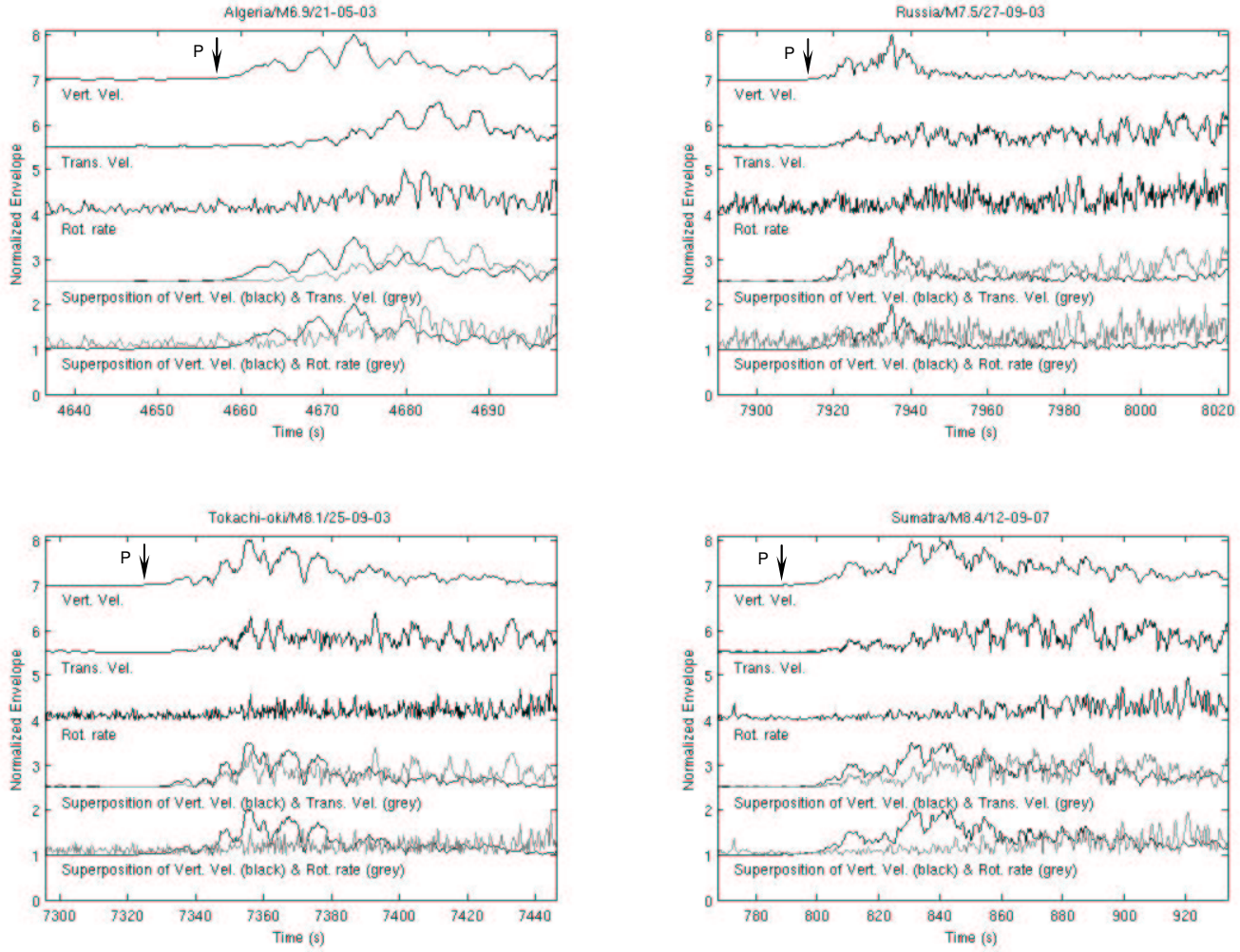

Figure 9. Normalized envelopes of individual seismograms and their superposition. For each subplot (from top, respectively): normalized envelopes of vertical and transverse components of ground velocity, vertical component of rotation rate, and the superposition of the envelopes of vertical and transverse velocities, and of vertical velocity and rotation rate.

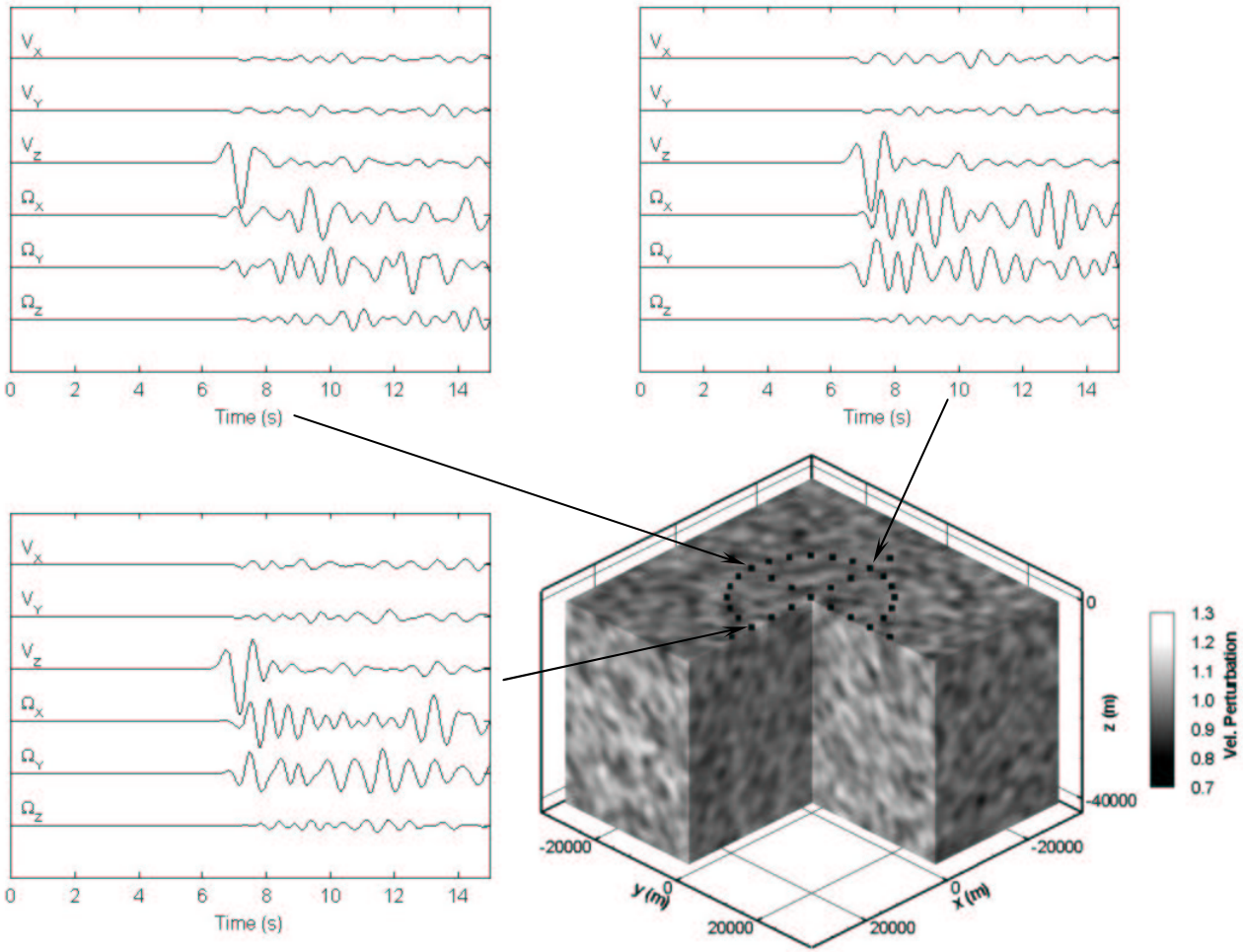

Figure 10. Schematic illustration of a 3D Von Kármán random medium used in this study (correlation length a = 2000m, root-mean square perturbation of V_S is 6.51%) and 6-component-seismograms obtained at three different receivers for a plane P wave propagating upward (in a vertical direction) from the bottom of the model. For each set of translational velocities (V_x, V_y, V_z) or rotation rates (Ω_x, Ω_y, Ω_z) amplitudes are scaled.

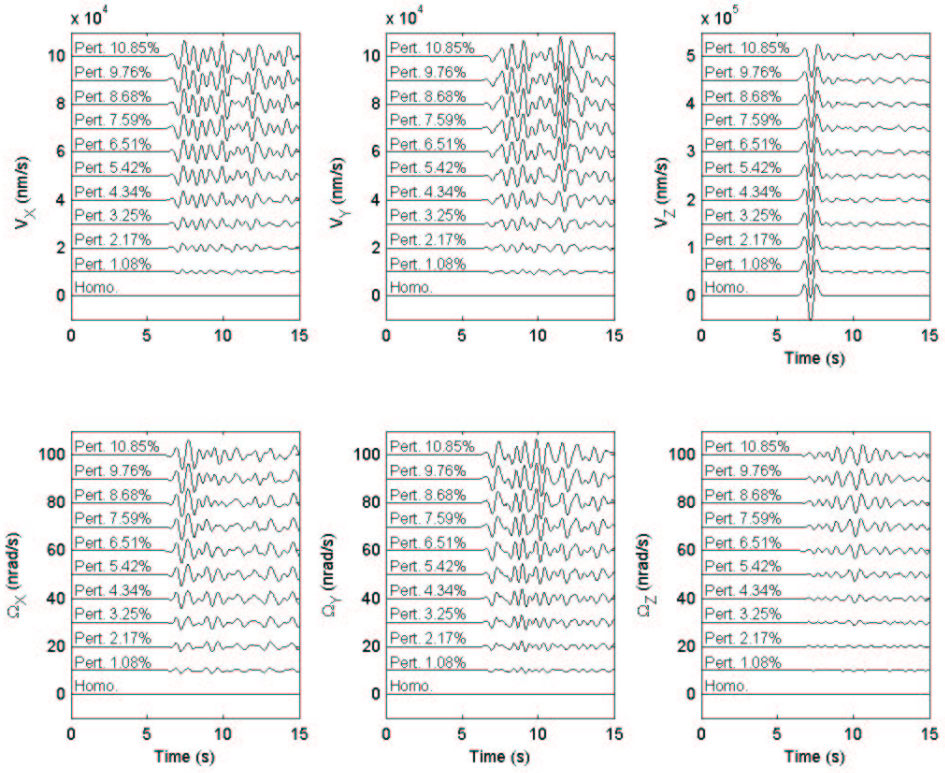

Figure 11. Variations of 6-component-seismograms obtained at one receiver as a function of velocity perturbation of the random medium (correlation length is fixed at 2000m) when a plane P wave propagates upward (in vertical direction) from the bottom of the model.

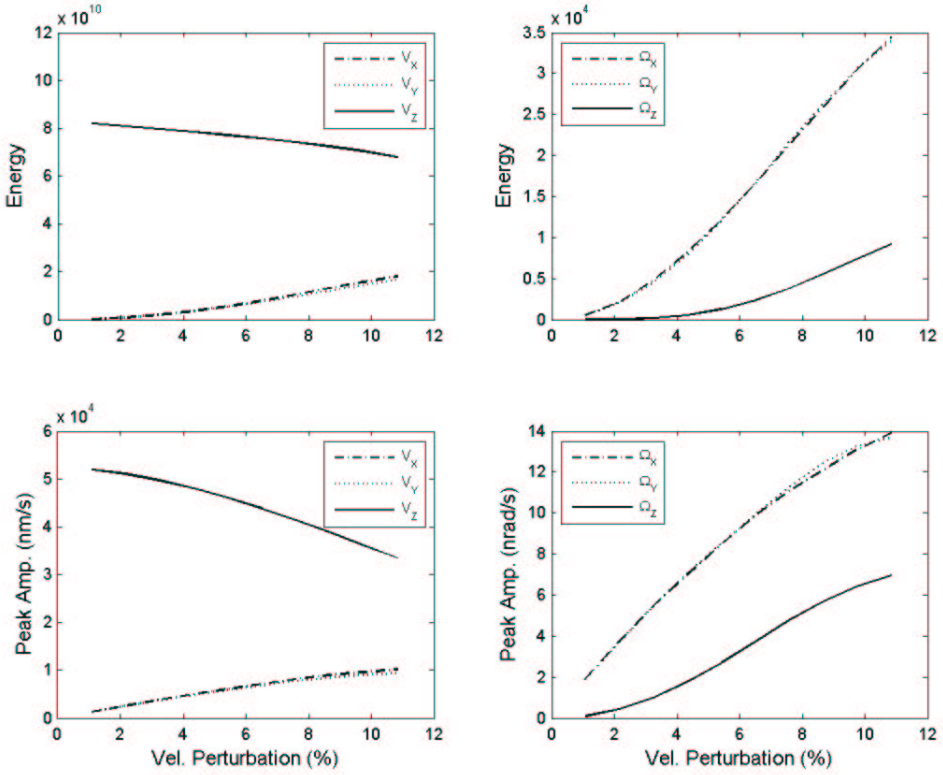

Figure 12. Variations of (the average values of) energy and peak amplitude of each translation and rotation component (calculated from 21s seismograms of 24 receivers distributed regularly around a circle of radius 15km from the center point at the surface of the model – figure 10) as a function of velocity perturbation of the random medium (correlation length is fixed to 2000m) when a plane P wave propagates upward (in vertical direction) from the bottom of the model.

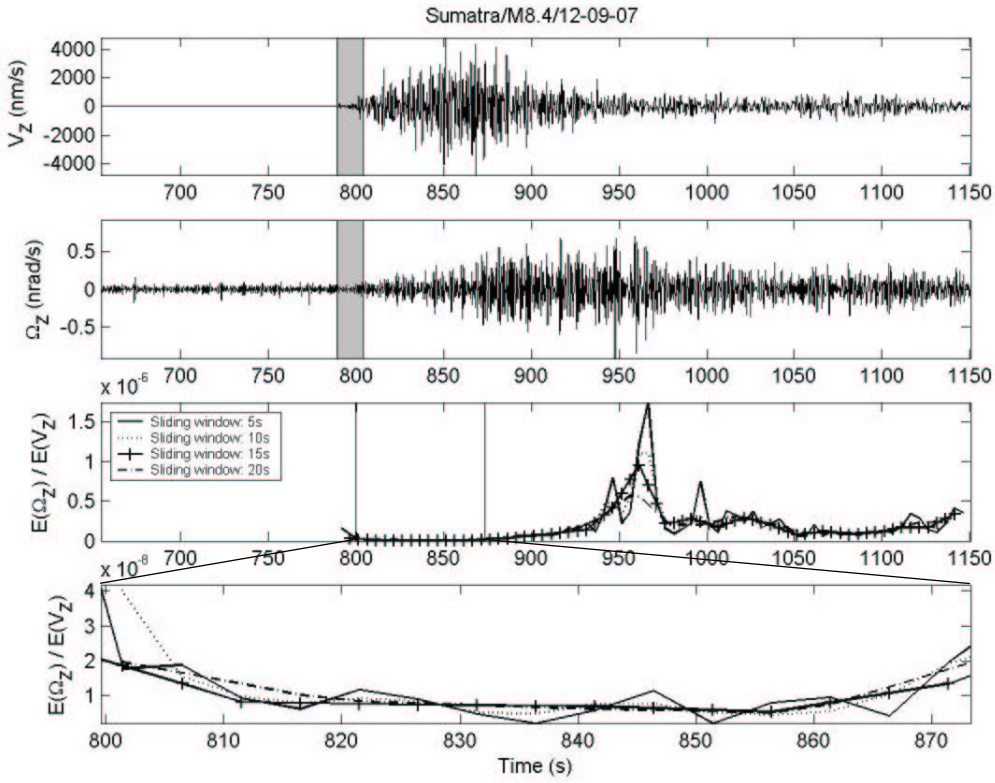

Figure 13a. Two top traces: Vertical components of velocity and rotation rate (respectively) in the P coda of the Sumatra event 12-09-2007, M8.4 after band-pass filtering between 0.5s and 1.5s. Two bottom traces: Ratio between energy of rotation rate and energy of vertical velocity calculated for time windows (illustrated by the vertical gray bands in the top traces) of different lengths, starting from the onset of P and sliding along the time series up to the end of the P coda.

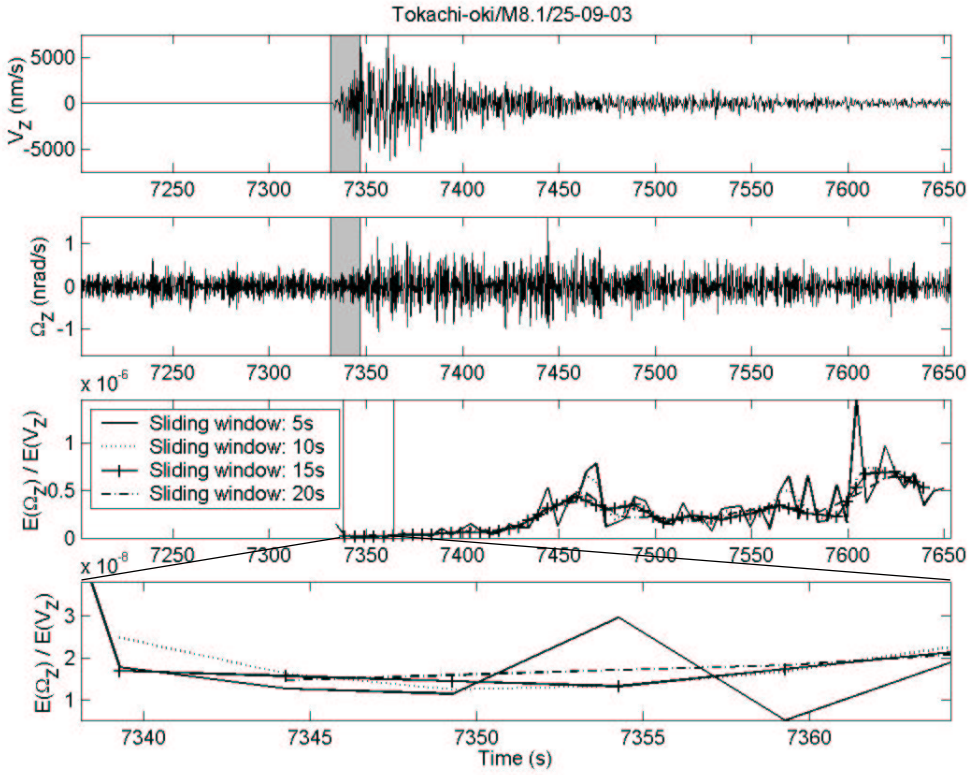

Figure 13b. Two top traces: Vertical components of velocity and rotation rate (respectively) in the P coda of the Tokachi-oki event 25-09-2003, M8.1 after band-pass filtering between 0.5s and 1.5s. Two bottom traces: Ratio between energy of rotation rate and energy of vertical velocity calculated for time windows (illustrated by the vertical gray bands in the top two traces) of different lengths, starting from the onset of P and sliding along the time series up to the end of the P coda.

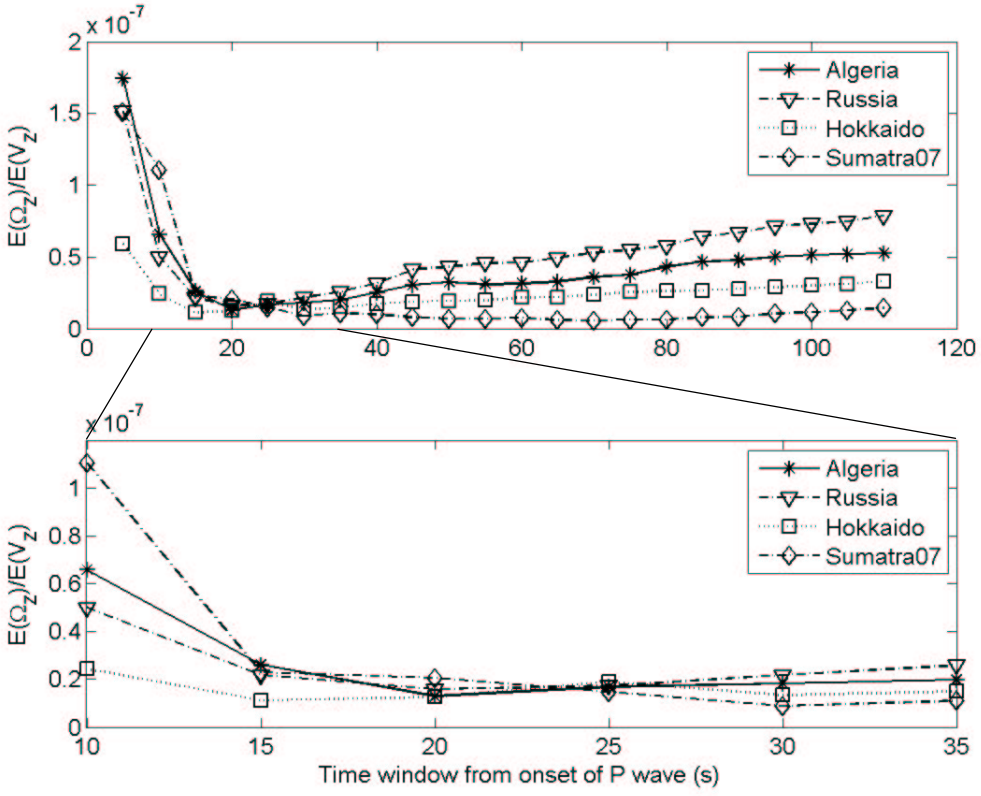

Figure 14. Ratios between energy of rotation rate and energy of vertical velocity in typical events calculated for different time windows. All the time windows start at the onset of direct P waves and their lengths are given by the horizontal axis.

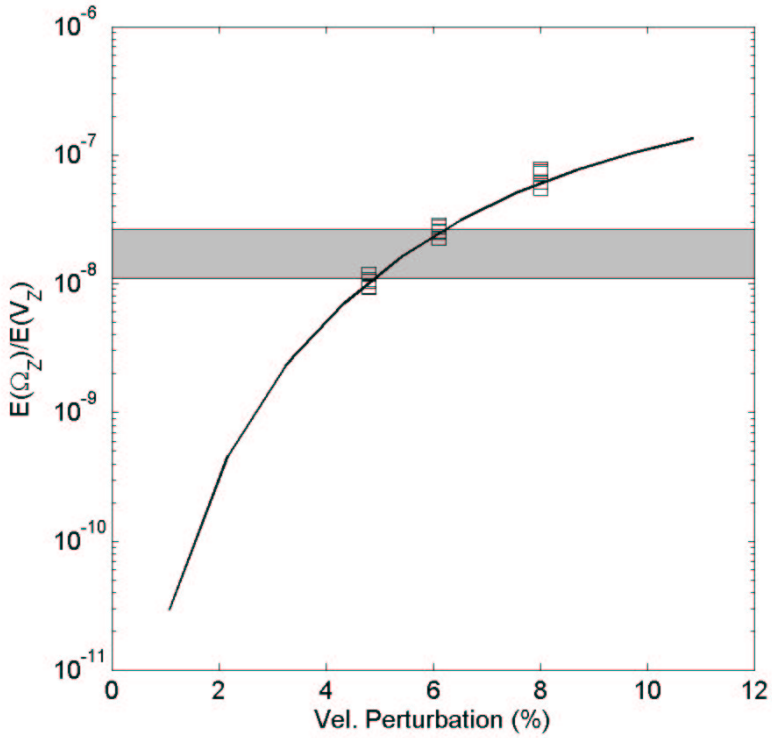

Figure 15. Comparison of observed and simulated energy ratios. Black curve: the (average) energy ratio as a function of velocity perturbation calculated from simulated seismograms (correlation length fixed at 2000m); Squares: the (average) energy ratio as a function of correlation length (from 1000m up to 15000m) obtained from simulations; Horizontal gray band: range of the energy ratios obtained from observations.